Applied Catalysis B: Environmental 168-169 (2015) 396–407

Contents lists available at ScienceDirect

Applied Catalysis B: Environmental

journal homepage: www.elsevier.com/locate/apcatb

Investigation of spillover effect in hydrotreating catalysts based on Co_2Mo_{10}− heteropolyanion and cobalt sulphide species

Al. A. Pimerzin*, P.A. Nikulshin, A.V. Mozhaev, A.A. Pimerzin, A.I. Lyashenko

Samara State Technical University, 244, Molodogvardiyskaya st., Samara 443100, Russia

ARTICLE INFO

Article history:
Received 10 October 2014
Received in revised form
15 December 2014
Accepted 21 December 2014
Available online 9 January 2015

Keywords:
Hydrotreating
Heteropolycompounds
Co_9S_8
CoMoS
Hydrogen spillover

ABSTRACT

$Co_2Mo_{10}/Co_x/Al_2O_3$ catalysts were synthesized from the ammonium salt of $[Co_2Mo_{10}O_{38}H_4]^{6-}$ anion supported on alumina modified with various amount of cobalt sulphide. The catalysts were analyzed using X-ray powder diffraction, N_2 physisorption, high-resolution transmission electron microscopy and X-ray photoelectron spectroscopy. The catalysts were tested in the hydrodesulphurization (HDS) of dibenzothiophene and 4,6-dimethyldibenzothiophene and the hydrodenitrogenation (HDN) of quinoline. The presence of cobalt sulphide particles on the catalysts surface affects catalytic properties significantly, whereas the structure of the active phase remains constant. The catalytic activity, selectivity and turnover frequency during the HDS and HDN reactions depend on the amount of modifier (cobalt sulphide) in the Co_x/Al_2O_3 supports and can be explained by hydrogen spillover effect. The model of HDS reaction over $Co_2Mo_{10}/Co_x/Al_2O_3$ catalyst involving hydrogen spillover was established. The obtained results allow us to focus attention on the role of the cobalt sulphide particles on the surface of hydrotreating catalysts.

1. Introduction

Heteroorganic compounds present in motor fuels are severe environmental contaminants and have bad influence on human health [1]. Gasoline exhaust remains are classified as “possible” carcinogen [2]. In this regard, countries all over the world have introduced stringent requirements on the pollutants (sulphur–, nitrogen–containing and polycyclic aromatic compounds) content in motor fuels. The 15 ppm sulphur specification for ultra low sulphur diesel (ULSD) fuel has been introduced in the USA since 2007 as well as “Sulphur-free” diesel and gasoline fuels with S content ≤10 ppm have become mandatory in European Union since 2009. According to Brazilian ecological requirements, the amount of sulphur in diesel has been limited to 10 ppm since 2013 [3,4]. Along with that new European regulations [5] will set tighter emission limits, known as Euro 5 and Euro 6, of atmospheric pollutants such as particulates and nitrogen oxide.

The hydrotreating (HDT) of petroleum fractions is the central refining process in order to produce clean fuels that meets the actual ecological requirements. The major way to improve effectiveness of hydrotreating process is the development of new hydrodesulphurization (HDS) catalysts. For this purpose, the studies devoted to the HDS catalysts development raise considerable interest [6–8]. The major part of industrial HDT catalysts are supported $Co(Ni)Mo(W)/Al_2O_3$ systems, which can contain other elements. Today it is a well-known fact that the active phase of HDT catalysts is composed of molybdenum disulphide (MoS_2) promoted with cobalt and/or nickel atoms [9–12]. Various approaches aimed at changing the active phase composition, the promoter/molybdenum ratio, and the support nature were proposed to improve the catalytic properties [12–16].

Recently heteropolycompounds (HPCs) have been widely used as precursors of the active phase of the HDS catalysts. Different types of HPCs with Keggin [17–20] or Anderson [17,20–29] structures were proposed as precursors instead of commonly used ones. The main advantage of HPCs over conventional precursors is the presence of promoter 3d-metal as a heteroatom in heteropolyanion (HPA) that provides the molecular contact between Mo and promoter. The HPCs composition and heteroatom nature determined the final catalytic properties of the HDS catalysts [17,20,25,30]. The use of HPAs with higher Co/Mo ratio than in Anderson type XMo_6HPA leads to enhancement of the promoting effect in CoMo catalysts [17,24,28,30–34]. However, the use of HPAs does not allow to increase the Co/Mo ratio up to optimal 0.5 value [7,8]. Previously it was shown that catalysts prepared with Co_2Mo_{10}HPA demonstrate better results in the HDS reactions than other counterparts [24,29,30,34,35]. Improved catalytic properties of the catalysts prepared with the Co_2Mo_{10}HPA are caused by the active phase

* Corresponding author. Tel.: +7 846 242 3580; fax: +7 846 242 3580.
E-mail address: al.pimerzin@gmail.com (Al.A. Pimerzin).

http://dx.doi.org/10.1016/j.apcatb.2014.12.031
0926-3373/

morphology and composition. The use of Co_2Mo_{10}HPA provides an opportunity to prepare HDS catalysts with highly effective active sites with enhanced TOF values [26]. In spite of high performance of CoMo active sites formed from Co_2Mo_{10}HPA integral activity of the HDS catalysts might not be enough to produce ULSD at conventional conditions. Hence, a lot of studies are focused on improving catalytic properties of the sulphide CoMo-catalysts.

Numerous researches are aimed at improving the catalytic properties of the catalysts prepared with HPCs. Higher values of the promotion ratio in the catalysts can be reached using various organic additives and chelating agents [26–28,36,37] or by modifying the catalyst support with promoter metals [38–41]. Nonmetal and noble metal modifiers were also investigated in order to improve catalytic properties of the HDT catalysts [42–47]. The synergetic effect was discovered during the investigation of the support surface modification with transition metals [41]. This synergism was related to the hydrogen spillover effect that was previously observed in HDT reactions over transition metal sulphides [48–51].

For the first time the effect of hydrogen atoms migration from the metal particles to the support and over it was described in 1969. Boudart et al. called this effect as "spillover", because hydrogen atoms spill over from a hydrogen-rich to a hydrogen-poor surface [52]. Hydrogen spillover effect in HDT reactions is usually investigated in stacked bed reactor with separated layers of the catalysts [48,49,53–57]. It has already been shown that cobalt sulphide can play the role of spillover hydrogen donor, whereas MoS_2 – that of acceptor [41,48–50,58]. However, the influence of spillover effect on action of promoted CoMo sites has not been investigated yet. The objective of the research was to investigate the effect of the modifying alumina surface with cobalt sulphide on the physicochemical characteristics of the CoMoS active phase formed from Co_2Mo_{10}HPA as well as catalytic properties of the $Co_2Mo_{10}/Co_x/Al_2O_3$ catalysts. Moreover, the role of cobalt sulphide particles on the surface of alumina supported CoMo-catalysts and the assumption about hydrogen spillover over catalyst surface from cobalt sulphide particles to CoMoS phase crystallites were studied.

2. Experimental

2.1. Supports and catalysts preparation

Commercial sample of alumina (from Novokuibyshevsk Catalyst Factory, specific surface area (SSA) 220 m^2/g, pore volume 0.74 cm^3/g, effective pore radius 31.5 Å) was used in this work.

Co-modified carriers Co_x/Al_2O_3, where x (over the 0–10.0 wt.% range) is the Co-loading, were prepared by wetness impregnation of commercial alumina with Co (II) nitrate aqueous solutions. The impregnated samples were dried at 60, 80, and 110 °C (for 2 h at each temperature) and sulphided at 400 °C (2 h) in H_2S/H_2 atmosphere (15 vol.% H_2S, flow rate is 4.0 L/h).

Ammonium salt of decamolybdodicobaltate $(NH_4)_6[Co_2Mo_{10}O_{38}H_4] \times 7H_2O$ (Co_2Mo_{10}Am) was prepared in accordance with the published procedures [59]. To confirm the composition and structure of HPC its elemental analysis was performed and IR spectra are recorded according to Nikulshin et al. [60].

$Co_2Mo_{10}/Co_x/Al_2O_3$ catalysts were prepared by impregnation of modified carriers with aqueous solutions containing the required amounts of Co_2Mo_{10}Am. The calculated amount of Mo in the catalysts was 12.7 wt.%. The total amount of Co in the catalysts depended on the Co-loading in the Co_x/Al_2O_3 supports used. Then impregnated samples were dried (60, 80, and 110 °C for 2 h) without further calcination.

2.2. Characterization of prepared samples

2.2.1. Supports and catalysts textural properties

Textural characteristics of the prepared supports and catalysts were determined by nitrogen adsorption at 77 K on a Quantochrome Autosorb-1 adsorption porosimeter. The SSA was calculated using the Brunauer–Emmett–Teller method at relative partial pressure P/P_0 of 0.05–0.3. The total pore volume and pore size distribution were measured by a desorption curve using the Barret–Joyner–Halenda model at relative partial pressure P/P_0 of 0.99. The samples were vacuum-dried before the adsorption measurement at 350 °C for 6 h at $p < 10^{-1}$ Pa.

2.2.2. X-ray diffraction (XRD)

The X-ray diffraction (XRD) patterns were obtained on a ARLX'-TRA Powder Diffractometer with Cu Kα radiation (λ = 1.54056 Å), 38 mA, 43 kV with a scanning speed of 2°/min. Powders were loaded on the glass disk by packing the samples into a cavity on this disk. Obtained diffractograms were analyzed using the standard JCPDS files.

2.2.3. High resolution transmission electron microscopy (HRTEM)

HRTEM images of the MoS_2 catalysts were obtained on a Tecnai G2 20 electron microscope with lattice–fringe resolution 0.14 nm at accelerating voltage 200 kV. The high resolution images of periodic structures were analyzed by the Fourier method. A local energy-dispersive X-ray analysis (EDAX) was carried out on an EDAX spectrometer fitted with a Si (Li) detector with resolution 130 eV. The samples examined by HRTEM were prepared on a perforated carbon film mounted on a copper grid.

The average length of the slab ($\bar{L}$) and the stacking degree ($\bar{N}$) were calculated and averaged using the data obtained from 8 to 10 TEM micrographs (an equivalent of at least 400 crystallites) for each catalyst. The average length ($\bar{L}$) approximately corresponds to the diagonal dimension of the observed MoS_2 platelet. The dispersion of edge and corner Mo atoms (denoted as D) was also calculated. In this calculation, it was assumed that MoS_2 is a perfect hexagon in accordance with Kasztelan et al. [61]. The D value was statistically evaluated by dividing the number of Mo atoms at the edge surface by the total number of Mo atoms using the crystallite sizes determined from HRTEM:

$$D = \frac{Mo_E + Mo_C}{Mo_T} = \frac{\underset{i=1..t}{\Sigma} 6n_i - 6}{\underset{i=1..t}{\Sigma} 3n_i^2 - 3n_i + 1} \quad (1)$$

where, Mo_E, Mo_C and Mo_T are numbers of Mo atoms located on edges, corners and total number, respectively, in average MoS_2 crystallite (evaluated from HRTEM), n_i is the number of Mo atoms along one side of the MoS_2 slab determined from its length and t is the total number of slabs in the TEM micrographs.

The average stacking degree ($\bar{N}$) was calculated by the following equation:

$$\bar{N} = \frac{\underset{i=1..t}{\sum} n_i N_i}{\underset{i=1..t}{\sum} n}, \quad (2)$$

where, n_i is the number of stacks in N_i layers.

2.2.4. X-ray photoelectron spectroscopy (XPS)

The XPS spectra were obtained on a Kratos Axis Ultra DLD spectrometer using monochromatic AlKα source ($h\nu$ = 1486.6 eV, 150 W). Analysis procedure described in details in [26,27]. $CoMo/Al_2O_3$ spectra decomposition technique used in this work was developed by Gandubert et al. [62,63].

The XPS decomposition allowed to determine the absolute quantification of each type of species:

$$C(j)_{\mathrm{T}}^{\mathrm{at}} = \frac{A_j/S_j}{\sum_{i=1..t} A_i/S_i} \times 100 \text{ and } C(j)_{\mathrm{T}} = \frac{\mathrm{Ar}_j \cdot A_j/S_j}{\sum_{i=1..t} (\mathrm{Ar}_i \cdot A_i/S_i)} \times 100 \quad (3)$$

where, $C(j)_{\mathrm{T}}^{\mathrm{at}}$ and $C(j)_{\mathrm{T}}$ are the j species concentrations on the catalyst surface in at.% and wt.%, respectively, A_i is the measured area of the species i, S_i is the sensitivity factor of the atom related to the species i (provided by the manufacturer) and Ar_i is the atomic weight of element.

The relative concentrations of each Co and Mo species (Co^{2+}, Co_9S_8, CoMoS, Mo^{6+}, MoS_xO_y and MoS_2) for every sulphided catalyst were determined. For example, the relative amount of CoMoS was determined using the following equation:

$$[\mathrm{CoMoS}](\mathrm{rel.\%}) = \frac{A_{\mathrm{CoMoS}}}{A_{\mathrm{CoMoS}} + A_{\mathrm{Co_9S_8}} + A_{\mathrm{Co^{2+}}}} \times 100, \quad (4)$$

where, A_X represents the peak area of species x.

The effective Co content in CoMoS phase (at.% and wt.%, respectively) was evaluated with the following equations:

$$C_{\mathrm{CoMoS}}^{\mathrm{at}} = [\mathrm{CoMoS}] \times C(\mathrm{Co})_T^{\mathrm{at}} \text{ and } C_{\mathrm{CoMoS}} = [\mathrm{CoMoS}] \times C(\mathrm{Co})_T, \quad (5)$$

where, $C(\mathrm{Co})_T^{\mathrm{at}}$ and $C(\mathrm{Co})_T$ represents the effective cobalt concentration (at.% and wt.%, respectively) on the surface of the catalysts obtained by XPS.

The effective Co content (wt.%) in a CoMoS species with a stacking number more than 1 (multi-slab) was determined using the following equation:

$$C'_{\mathrm{CoMoS}} = C_{\mathrm{CoMoS}} \times F_{\mathrm{multi-slab}}, \quad (6)$$

where, $F_{\mathrm{multi\text{-}slab}}$ is content of active phase particles with a stacking number more than 1 (from TEM measurements).

The total Co/Mo atomic ratio on the surface of catalysts was calculated from XPS according to the following equation:

$$(\mathrm{Co/Mo})_{\mathrm{tot}} = \frac{C(\mathrm{Co})_T^{\mathrm{at}}}{C(\mathrm{Mo})_T^{\mathrm{at}}}, \quad (7)$$

The promoter ratio in the average CoMoS crystallite was determined as follows:

$$(\mathrm{Co/Mo})_{\mathrm{slab}} = \frac{C_{\mathrm{CoMoS}}^{\mathrm{at}}}{C_{\mathrm{MoS_2}}^{\mathrm{at}}}, \quad (8)$$

where, C_X^{at} is the absolute concentration of Co (Mo) in the CoMoS (MoS_2) species (at.%).

The promoter ratio in the edges of CoMoS active phase crystallites was calculated by the following formula:

$$(\mathrm{Co/Mo})_{\mathrm{edge}} = \frac{(\mathrm{Co/Mo})_{\mathrm{slab}} \times \mathrm{Mo_T}}{\mathrm{Mo_E} + \mathrm{Mo_C}} = \frac{(\mathrm{Co/Mo})_{\mathrm{slab}}}{D}, \quad (9)$$

where, D is the dispersion edge and corner Mo atoms of the active phase (Eq. (1)).

Using XPS and HRTEM results the packing density of the active phase particles on the catalyst surface denoted as m (MoS_2 crystallites per 1000 nm^2) was calculated:

$$m = \frac{C_{\mathrm{MoS_2}} \cdot N_{\mathrm{A}}}{\mathrm{Mr_{Mo}} \cdot \mathrm{Mo_T} \cdot \mathrm{SSA} \cdot 10^{15}}, \quad (10)$$

where, $C_{\mathrm{MoS_2}}$ is the absolute concentration of Mo in the MoS_2 species (wt.%), N_{A} is the Avogadro constant (6.022×10^{23} mol^{-1}), $\mathrm{Mr_{Mo}}$ is the molar mass of molybdenum (95.95 g/mol), Mo_T is the total number of Mo atoms in average MoS_2 crystallite (evaluated from HRTEM and hexagonal model) and SSA is the specific surface area (m^2/g) of the catalyst.

2.3. Catalytic properties examination

2.3.1. Dibenzothiophene and 4,6-dimethyldibenzothiophene HDS over the prepared catalysts

HDS of dibenzothiophene (DBT) and 4,6-dimethyldibenzothiophene (4,6-DMDBT) were carried out using a fixed-bed micro reactor in a high-pressure flow system. A 0.1–0.5 g quantity of the catalyst (0.25–0.50 mm) was diluted with 1 cm^3 low surface area carborundum (0.25–0.50 mm) and placed into tube reactor. Prior to testing, the catalysts were activated by sulphidation with mixture of 6% DMDS in toluene (LHSV = 10 h^{-1}, 3 MPa) at 240 and 340 °C and for 10 h.

The DBT solution in toluene (1500 ppm of sulphur) or the 4,6-DMDBT solution in toluene (300 ppm of sulphur) was introduced into the reactor at 40 h^{-1} with hydrogen: feedstock ratio 600 NL/L at 250–275 °C and total pressure 3.0 MPa. Liquid product compositions of the samples collected at 0.5 h intervals were determined using a Crystall-5000 gas chromatograph equipped with a 30 m OV-101 column. The reaction products were identified by matching retention times with commercially available standards as well as by the gas chromatography–mass spectrometry analysis using Finnigan Trace DSQ. The HDS reaction was run for 10 h in order to evaluate the catalyst deactivation. However, all the catalysts exhibited stable performance and could achieve a steady state after 5–6 h.

The rate constant of the pseudo-first-order HDS reactions of DBT and 4,6-DMDBT were determined using the following equations:

$$k_{\mathrm{HDS}}^{\mathrm{DBT}} = -\frac{F_{\mathrm{DBT}}}{W} \ln(1 - x_{\mathrm{DBT}}) \text{ and } k_{\mathrm{HDS}}^{\text{4,6-DMDBT}} = -\frac{F_{\text{4,6-DMDBT}}}{W} \ln(1 - x_{\text{4,6-DMDBT}}), \quad (11)$$

where, $k_{\mathrm{HDS}}^{\mathrm{DBT}}$ and $k_{\mathrm{HDS}}^{\text{4,6-DMDBT}}$ are the pseudo-first order reaction constants for the HDS of DBT and 4,6-DMDBT (mol g^{-1} h^{-1}), respectively, x_{DBT} and $x_{\text{4,6-DMDBT}}$ are the DBT and 4,6-DMDBT conversions (%), respectively, $F_{\mathrm{DBT(4,6\text{-}DMDBT)}}$ is the reactant molar flow (mol h^{-1}) and W is the catalyst weight (g).

The products of DBT HDS were biphenyl (BP) from the direct desulphurization pathway (DDS) and cyclohexylbenzene (CHB) and bicyclohexyl (BCH) from the HYD pathway. Only traces of hydrogenated tetrahydro- and perhydrodibenzothiophenes were observed. According to the reaction network of DBT HDS (Scheme 1) HYD/DDS selectivity was calculated by the following equation:

$$\mathrm{Sel_{HYD/DDS}} = \frac{k_{\mathrm{HYD}}}{k_{\mathrm{DDS}}} = \frac{C_{\mathrm{CHB}} + C_{\mathrm{BCH}}}{C_{\mathrm{BP}}} \quad (12)$$

where, C_{CHB}, C_{BCH}, C_{BP} are CHB, BCH and BP concentrations in the reaction products, respectively (wt.%).

The products of the 4,6-DMDBT HDS included 3,3′-dimethylbiphenyl (3,3′-DMBP) via the DDS pathway, as well as 1-methyl-3-(2-methylphenyl) cyclohexane (methylcyclohexyltoluene (MCHT)) and 3,3′-dimethylbicyclohexyl (3,3′-DMBCH) via the HYD pathway. Only traces of the hydrogenated species (4,6-tetrahydro- and perhydrodibenzothiophenes) were observed. The HYD/DDS selectivity was calculated using the following equation according to the reaction network for the HDS of 4,6-DMDBT (Scheme 2):

$$\mathrm{Sel_{HYD/DDS}} = \frac{k_{\mathrm{HYD}}}{k_{\mathrm{DDS}}} = \frac{C_{\mathrm{MCHT}} + C_{\text{3,3′-DMBCH}}}{C_{\text{3,3′-DMBP}}}, \quad (13)$$

where CMCHT, $C_{\text{3,3′-DMBCH}}$ and $C_{\text{3,3′-DMBP}}$ are the concentrations (wt.%) of MCHT, 3,3′-DMBCH and 3,3′-DMBP in reaction products, respectively.

The HYD/DDS selectivities in HDS reactions were compared at 25% conversion of DBT and 10% of 4,6-DMDBT. The amount of catalyst (LHSV) was varied to achieve the equal conversions.

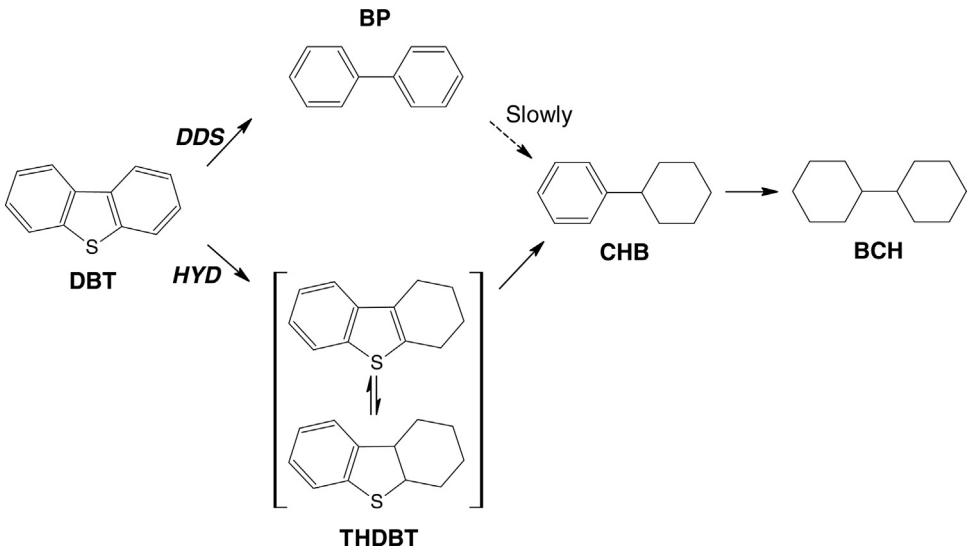

Scheme 1. Reaction network of HDS of DBT.

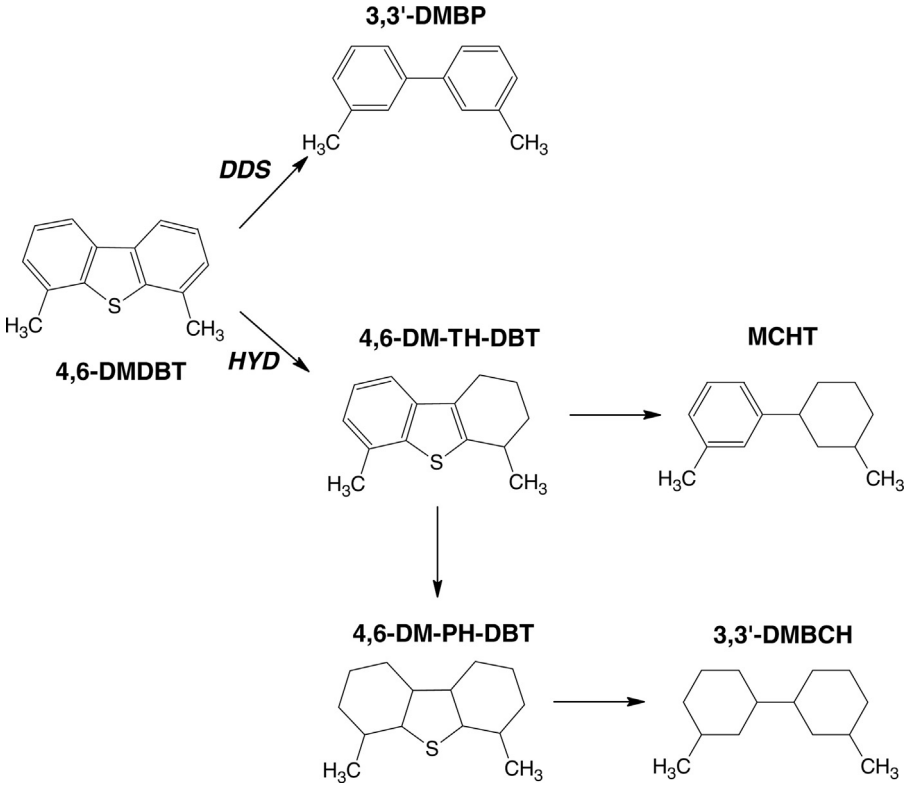

Scheme 2. Reaction network of HDS of 4,6-DMDBT.

Turnover frequencies (s^{-1}) for HDS of DBT and 4,6-DMDBT were calculated according to the equations:

$$\mathrm{TOF}_{\mathrm{HDS}} = \frac{F_{\mathrm{DBT}} \cdot x_{\mathrm{DBT}} \cdot \mathrm{Mr}_{\mathrm{Co}}}{W \cdot C_{\mathrm{CoMoS}} \cdot 3600} \text{ and } \mathrm{TOF}_{\mathrm{HDS}} = \frac{F_{\text{4,6-DMDBT}} \cdot x_{\text{4,6-DMDBT}} \cdot \mathrm{Mr}_{\mathrm{Co}}}{W \cdot C_{\mathrm{CoMoS}} \cdot 3600}, \quad (14)$$

where $F_{\mathrm{DBT(4,6\text{-}DMDBT)}}$ is the reactant molar flow (mol h^{-1}), x_{DBT} and $x_{\text{4,6-DMDBT}}$ are the DBT and 4,6-DMDBT conversions (%), respectively, W is the catalyst weight (g), C_{CoMoS} is the effective Co content (wt.%) in CoMoS phase and $\mathrm{Mr}_{\mathrm{Co}}$ is the molar mass of cobalt (58.9 g/mol).

The values of turnover frequencies ($\mathrm{TOF}^{/}$) on active sites located on the multi-layered CoMoS crystallites with average stacking number more than 1 were calculated as follows [26]:

$$\mathrm{TOF}^{/}_{\mathrm{HDS}} = \frac{F_{\mathrm{DBT}} \cdot x_{\mathrm{DBT}} \cdot \mathrm{Mr}_{\mathrm{Co}}}{W \cdot C^{/}_{\mathrm{CoMoS}} \cdot 3600} \text{ and } \mathrm{TOF}^{/}_{\mathrm{HDS}} = \frac{F_{\text{4,6-DMDBT}} \cdot x_{\text{4,6-DMDBT}} \cdot \mathrm{Mr}_{\mathrm{Co}}}{W \cdot C^{/}_{\mathrm{CoMoS}} \cdot 3600}, \quad (15)$$

where $C^{/}_{\mathrm{CoMoS}}$ is the effective Co content (wt.%) in a CoMoS species with a stacking number more than 1 (multi-slab).

Table 1
Composition and textural properties of prepared catalysts.

Catalyst	Amount in the catalyst (wt.%)		Textural properties of sulfided catalysts		
	Mo	Co (including carrier modifier)	SSA[a] (m^2/g)	Pore volume (cm^3/g)	APR[b] (Å)
Co_2Mo_{10}/Al_2O_3	12.7	1.6 (0.0)	140	0.28	31.6
$Co_2Mo_{10}/Co_{2.1}/Al_2O_3$	12.7	3.7 (2.1)	136	0.27	31.5
$Co_2Mo_{10}/Co_{4.1}/Al_2O_3$	12.7	5.7 (4.1)	134	0.26	31.6
$Co_2Mo_{10}/Co_{8.3}/Al_2O_3$	12.7	9.9 (8.3)	128	0.25	31.5

[a] Specific surface area.
[b] Average pore radius.

For the quantification of synergisms in $Co_2Mo_{10}/Co_x/Al_2O_3$ catalysts due to hydrogen spillover, a synergism factor (spillover effect – SE) was defined, which is expressed as:

$$SE = \frac{x_{Co_2Mo_{10}/Co_X/Al_2O_3}}{x_{Co_2Mo_{10}/Al_2O_3}} \quad (16)$$

where $x_{Co_2Mo_{10}/Al_2O_3}$ and $x_{Co\,2\,Mo_{10}/Co_X/Al_2O_3}$ are the DBT or 4,6-DMDBT conversions (%) in HDS over Co_2Mo_{10}/Al_2O_3 (reference sample) and modified $Co_2Mo_{10}/Co_x/Al_2O_3$ catalysts, respectively.

This approach was used previously in several works to characterize the stacked bed catalytic systems with separated beds of donor (**D**) and acceptor (**A**) of activated hydrogen [45,48,50,53–56,64].

In our case, it is better to use TOF values instead of conversions in order to account for changing the number of active sites on the catalyst surface. Therefore, the spillover effect based on turnover frequencies (SE^{TOF}) was also calculated:

$$SE^{TOF} = \frac{TOF_{Co_2Mo_{10}/Co_X/Al_2O_3}}{TOF_{Co_2Mo_{10}/Al_2O_3}} \quad (17)$$

where $TOF_{Co_2Mo_{10}/Al_2O_3}$ and $TOF_{Co_2Mo_{10}/Co_X/Al_2O_3}$ are the turnover frequency numbers for HDS of DBT or 4,6-DMDBT over Co_2Mo_{10}/Al_2O_3 (reference sample) and modified $Co_2Mo_{10}/Co_x/Al_2O_3$ catalysts, respectively.

The spillover synergism effect related to the multi-slab CoMoS species $SE^{/TOF}$ using $TOF^{/}$ values (similarly Eq. (17) was also calculated. That is why it became possible to evaluate the quantification of synergisms between Co_9S_8 and CoMoS particles on the catalyst surface.

2.3.2. Quinoline HDN over the prepared catalysts

HDN of Quinoline (Qui) was carried out by using a fixed-bed micro reactor in a high-pressure flow system described in 2.3.1. The Qui solution in toluene (750 ppm of nitrogen) was introduced into the reactor at 20 h^{-1} with the hydrogen: feedstock ratio 600 NL/L at 325 °C and total pressure 3.0 MPa. Liquid product compositions of the samples collected at 0.5 h intervals were determined with gas chromatography and mass spectrometry methods. The catalytic examination was run for 10 h in order to evaluate the catalyst deactivation.

The constant rate of the pseudo-first-order HDN reactions of Qui and the TOF values for Qui HDN were calculated with the equations described in 2.3.1. with the only difference that extent of denitrogenation was used instead of reactant conversion (similarly Eq. (11) and (14)).

3. Results

3.1. Prepared catalysts physicochemical characteristics

Alumina modifying with Co (up to 8.3 wt.%) has negligibly effect on textural characteristics of the sulphided catalysts (Table 1). The values of pore volume and average pore radius are kept similar for the catalysts prepared with modified supports as well as initial alumina. The SSA of the catalysts supported on modified carriers is 4–12 m^2/g smaller than the reference one.

XRD patterns of $Co_2Mo_{10}/Co_x/Al_2O_3$ catalysts after sulphidation procedures are shown in Fig. 1. The XRD patterns of the samples demonstrate only low temperature phase of γ-Al_2O_3 support. All the prepared catalysts have not shown Mo and Co XRD patterns. It is suggested that Mo and Co species are probably in X-ray amorphous state or the crystallites are too small to give XRD signals, though $Co_2Mo_{10}/Co_{8.3}/Al_2O_3$ catalyst contains an appreciable quantity of Co_9S_8 phase.

The chemical surface composition of the sulphided catalysts was evaluated by XPS.

The Mo 3d and Co 2p XPS spectra of the sulphided $Co_2Mo_{10}/Co_x/Al_2O_3$ catalysts are shown in Fig. 2. The Mo spectra exhibit Mo $3d_{5/2}$ peak at 228.8 eV characteristic of MoS_2. The Co $2p_{3/2}$ peak observed at approximately 778.6 eV in Co spectra characterize the cobalt sulphide (Co_9S_8). The peak at binding energy of 226.1 eV is assigned to sulphur (S 2s). In S 2p spectra, the BE = 161.6 ± 0.1 eV peak is a characteristic of sulphides containing sulphur in the form of S^{2-}. The obtained results of binding energy are in good agreement with the reported values [26,62,65–67]. All the XPS data and results of spectra decomposition are listed in Table 2. Increasing the Co loading in alumina affected the cobalt species allocation, whereas distribution of molybdenum particles remained constant for all the catalysts, with the Mo content in the MoS_2 particles equal to ~73 rel.%. The reference Co_2Mo_{10}/Al_2O_3 catalyst demonstrated the highest relative percentage of Co in the CoMoS phase (63 rel.%) and cobalt oxide species (35 rel.%), coupled with the absence of Co_9S_8 particles. The addition of cobalt to alumina increased the Co_9S_8 phase content in the catalysts from 2 to 70 rel.%. This growth was accompanied by the lowering of the relative concentration of CoMoS phase and cobalt oxide species. The total Co/Mo atomic ratio in the prepared catalysts varied from 0.23 to 1.14. Meanwhile the Co/Mo ratios in the CoMoS slabs and edges were approximately the same for different catalysts (0.20 and 0.75, respectively). The surface Co/Al atomic ratio in the catalysts increased from 0.045 to 0.144, whereas bulk Co/Al ratio grew from 0.018 to 0.119. The XPS results allowed to calculate the effective Co content in CoMoS phase species (C_{CoMoS}) and multi-slab CoMoS phase species having a stacking number more than 1 ($C^{/}_{CoMoS}$) (Table 2). The effective

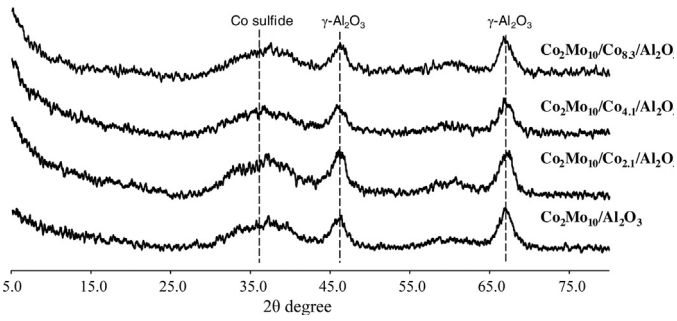

Fig. 1. X-ray diffraction patterns of sulfided $Co_2Mo_{10}/Co_x/Al_2O_3$ catalysts.

Table 2
Metal distribution for cobalt and molybdenum species present at the surface of sulfided catalysts.

Catalyst	$(Co/Mo)_{tot}$ [a]	$(Co/Mo)_{slab}$ [b]	$(Co/Mo)_{edge}$ [c]	C_{CoMoS} [d] (wt.%)	C'_{CoMoS} [e] (wt.%)	Co distribution (rel.%)			Mo distribution (rel.%)		
						CoMoS	Co_9S_8	Co^{2+}	MoS_2	MoS_xO_y	Mo^{6+}
Co_2Mo_{10}/Al_2O_3	0.23	0.20	0.76	1.62	0.48	63	2	35	73	14	13
$Co_2Mo_{10}/Co_{2.1}/Al_2O_3$	0.63	0.20	0.73	1.49	0.59	23	48	29	73	16	11
$Co_2Mo_{10}/Co_{4.1}/Al_2O_3$	0.87	0.21	0.76	1.18	0.57	17	64	19	70	18	13
$Co_2Mo_{10}/Co_{8.3}/Al_2O_3$	1.14	0.18	0.67	1.02	0.51	12	70	18	76	13	11

[a] Co/Mo total atomic ratio calculated from XPS results (Eq. (7)).
[b] Co/Mo ratio in the CoMoS active phase slabs calculated from XPS results (Eq. (8)).
[c] Co/Mo ratio on the edges of CoMoS active phase calculated from XPS and HRTEM results (Eq. (9)).
[d] Effective Co content in total CoMoS phase species from XPS results (Eq. (5)).
[e] Effective Co content in multi-slab CoMoS phase species having stacking number more than 1 (Eq. (6)).

Co content in total CoMoS phase species decreased from 1.62 to 1.02 wt.% and effective Co content in multi-slab CoMoS phase species varied only slightly near 0.55 wt.% with cobalt addition to support.

Representative HRTEM micrographs of sulphided $Co_2Mo_{10}/Co_x/Al_2O_3$ catalysts are shown in Fig. 3. The average length (obtained by HRTEM) of CoMoS phase varies from 2.6 to 2.9 nm and average stacking number in MoS_2 crystallites equals to 1.4–1.7 (Table 3). Increasing the cobalt content in alumina has no effect on the packing density of the active phase particles on the catalyst surface, meanwhile the particles distribution on stacking number changes. The CoMoS particles distribution over size of crystallites was the same for all $Co_2Mo_{10}/Co_x/Al_2O_3$ catalysts. The amount of multi-slab CoMoS particles (with stacking number more than 1) increased with cobalt content enrichment catalysts, having its maximum that is equal to a half (50 rel.%) for $Co_2Mo_{10}/Co_{8.3}/Al_2O_3$ catalyst. Dispersion of Mo edge and corner atoms in CoMoS phase particles remained constant and was equal to 0.41 for all the samples. The packing density of the active phase particles on the catalyst surface varies between 44 and 51 MoS_2 crystallites per 1000 nm^2 for all catalysts.

3.2. Catalytic properties of the synthesized catalysts

The results of DBT HDS on $Co_2Mo_{10}/Co_x/Al_2O_3$ catalysts are presented in Table 4. The DBT conversion increases (from 21 to 36% at 250 °C and from 31 to 49% at 275 °C) with cobalt addition, reaching a maximum at 4.1 wt.% and above of cobalt in the carrier. The values of selectivity ratio $Sel_{HYD/DDS}$ are 0.05–0.06 for 250 °C and 0.08–0.11 for 275 °C. TOF values for HDS DBT were remarkable and grew with the addition of cobalt sulphide on the catalyst surface. TOF numbers grew from 3.5 to 9.4×10^{-4} s^{-1} at 250 °C and grew from 5.1 to 12.7×10^{-4} s^{-1} at 275 °C.

The results of catalytic activity measurement in 4,6-DMDBT HDS over prepared catalysts are summarized in Table 5. The values of reaction rate constants have one order less than for DBT HDS. The increase of Co content in the support gave a rise to the 4,6-DMDBT conversion from 5% to 11% and selectivity ratio ($Sel_{HYD/DDS}$) from 5.5 to approximately 7.5. The TOF value for 4,6-DMDBT HDS on Co_2Mo_{10}/Al_2O_3 was 0.13×10^{-4} s^{-1} whereas TOF number for cobalt modified catalyst amounted to 0.45×10^{-4} s^{-1}.

Table 6 shows the results of Qui HDN investigation. Qui conversion slowly increased as support was modified with cobalt sulphide from 35% (for reference Co_2Mo_{10}/Al_2O_3 catalyst) to 42% (for $Co_2Mo_{10}/Co_{8.3}/Al_2O_3$ catalyst), whereas the TOF values were almost doubled (from 5.8 to 10.9×10^{-4} s^{-1}) with cobalt addition to the alumina.

4. Discussion

The reported decrease of SSA of the catalysts supported on modified carriers is 4–12 m^2/g. It can be caused by formation of Co_3O_4

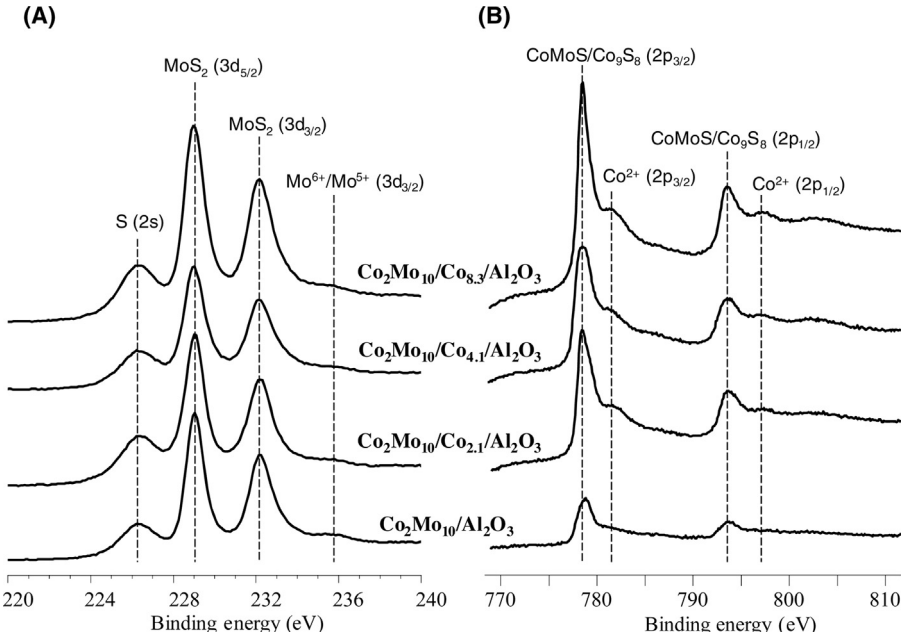

Fig. 2. XPS spectra of sulfided $Co_2Mo_{10}/Co_x/Al_2O_3$ catalysts. (A) Mo 3d spectra, (B) Co 2p spectra.

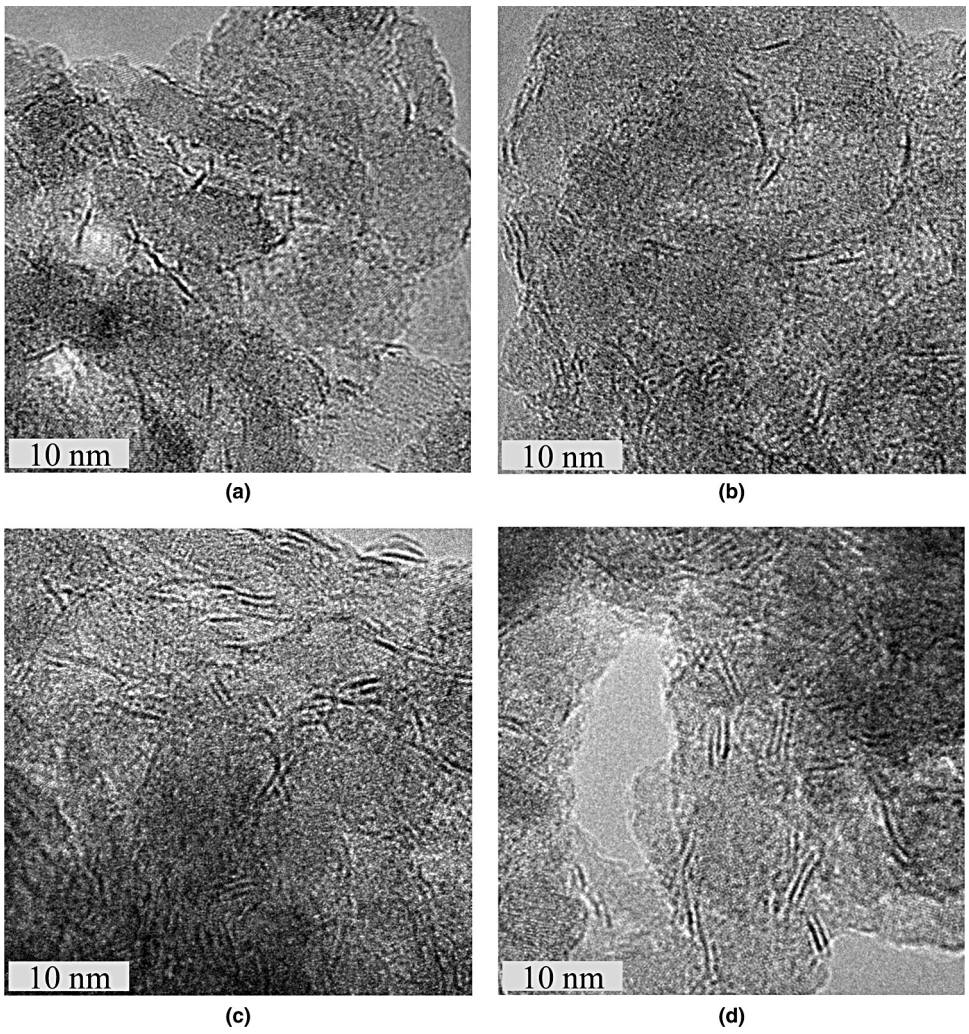

Fig. 3. HRTEM micrographs of sulfided catalysts: (a) Co_2Mo_{10}/Al_2O_3, (b) $Co_2Mo_{10}/Co_{2.1}/Al_2O_3$, (c) $Co_2Mo_{10}/Co_{4.1}/Al_2O_3$, (d) $Co_2Mo_{10}/Co_{8.3}/Al_2O_3$.

Table 3
Morphological characteristics of the CoMoS active phase for $Co_2Mo_{10}/Co_{x.x}/Al_2O_3$ catalysts calculated from TEM micrographs.

Catalyst	$\bar{L}$(nm)	$\bar{N}$	D[a]	Distribution of slab length (rel.%)				Distribution of stacking number (rel.%)			
				<2 nm	2.4 nm	4.6 nm	>6 nm	1	2	3	>3
Co_2Mo_{10}/Al_2O_3	2.9	1.4	0.40	21	65	12	2	71	24	4	1
$Co_2Mo_{10}/Co_{2.1}/Al_2O_3$	2.7	1.5	0.41	25	64	10	1	60	33	6	1
$Co_2Mo_{10}/Co_{4.1}/Al_2O_3$	2.6	1.7	0.43	29	61	9	1	52	36	11	1
$Co_2Mo_{10}/Co_{8.3}/Al_2O_3$	2.7	1.7	0.41	25	64	10	1	50	34	14	2

[a] Dispersion of Mo edge and corner atoms (Eq. (1)).

Table 4
Catalytic properties of $Co_2Mo_{10}/Co_{x.x}/Al_2O_3$ catalysts in DBT HDS under the following reaction conditions: T = 250, 275 °C, P = 3.0 MPa, LHSV = 40 h^{-1}, H_2/feedstock = 600 NL/L.

Catalyst	T (°C)	x (%)	Rate constants × 10^4 (mol h^{-1} g^{-1})			Selectivity ratio, $Sel_{HYD/DDS}$	TOF × 10^4 (s^{-1})	TOF/ × 10^4 (s^{-1})	SE[TOF a]	SE/[TOF b]
			k_{HDS}	k_{DDS}	k_{HYD}					
Co_2Mo_{10}/Al_2O_3	250	21	3.8	3.6	0.2	0.048	3.5	11.7	–	–
$Co_2Mo_{10}/Co_{2.1}/Al_2O_3$		25	4.6	4.4	0.2	0.052	4.4	11.2	1.3	1.0
$Co_2Mo_{10}/Co_{4.1}/Al_2O_3$		34	6.7	6.3	0.4	0.065	7.6	15.9	2.2	1.4
$Co_2Mo_{10}/Co_{8.3}/Al_2O_3$		36	7.2	6.8	0.4	0.063	9.4	18.7	2.7	1.6
Co_2Mo_{10}/Al_2O_3	275	31	6.0	5.5	0.5	0.083	5.1	17.2	–	–
$Co_2Mo_{10}/Co_{2.1}/Al_2O_3$		39	7.9	7.3	0.6	0.088	6.9	17.3	1.4	1.0
$Co_2Mo_{10}/Co_{4.1}/Al_2O_3$		50	11.3	10.2	1.1	0.105	11.3	23.5	2.2	1.4
$Co_2Mo_{10}/Co_{8.3}/Al_2O_3$		49	10.9	9.8	1.1	0.110	12.7	25.4	2.5	1.5

[a] Synergism effect based on turnover frequencies (Eq. (17)).
[b] Synergism effect based on turnover frequencies related to multi-slab CoMoS species.

Table 5
Catalytic properties of $Co_2Mo_{10}/Co_{x,x}/Al_2O_3$ catalysts in HDS of 4,6-DMDBT at T = 275 °C, P = 3.0 MPa, LHSV = 40 h^{-1}, H_2/feedstock = 600 NL/L.

Catalyst	T (°C)	x (%)	Rate constants × 10^4 (mol h^{-1} g^{-1})			Selectivity ratio, $Sel_{HYD/DDS}$	TOF × 10^4 (s^{-1})	TOF$^{/}$ × 10^4(s^{-1})	SE^{TOF}[a]	SE$^{/TOF}$[b]
			k_{HDS}	k_{DDS}	k_{HYD}					
Co_2Mo_{10}/Al_2O_3	275	5.0	0.17	0.026	0.14	5.5	0.13	0.45	–	–
$Co_2Mo_{10}/Co_{2.1}/Al_2O_3$		5.5	0.18	0.028	0.16	5.6	0.14	0.43	1.1	1.0
$Co_2Mo_{10}/Co_{4.1}/Al_2O_3$		10.0	0.34	0.045	0.30	6.7	0.45	0.94	3.4	2.1
$Co_2Mo_{10}/Co_{8.3}/Al_2O_3$		11.0	0.38	0.045	0.33	7.5	0.47	0.94	3.6	2.1

[a] Synergism effect based on turnover frequencies (Eq. (17)).
[b] Synergism effect based on turnover frequencies related to multi-slab CoMoS species.

Table 6
Catalytic properties of $Co_2Mo_{10}/Co_{x,x}/Al_2O_3$ catalysts in HDN of Quinoline at T = 325 °C, P = 3.0 MPa, LHSV = 20 h^{-1}, H_2/feedstock = 600 NL/L.

Catalyst	T (°C)	x (%)	k_{HDN} × 10^4(mol h^{-1} g^{-1})	TOF × 10^4 (s^{-1})	TOF$^{/}$ × 10^4 (s^{-1})	SE^{TOF}	SE$^{/TOF}$p4.5pc
Co_2Mo_{10}/Al_2O_3	325	35	4.0	5.8	18.1	–	–
$Co_2Mo_{10}/Co_{2.1}/Al_2O_3$		40	4.7	7.1	17.9	1.2	1.0
$Co_2Mo_{10}/Co_{4.1}/Al_2O_3$		39	4.6	8.8	18.2	1.5	1.0
$Co_2Mo_{10}/Co_{8.3}/Al_2O_3$		42	5.1	10.9	21.8	1.9	1.2

and, further, Co sulphide species. The bulk and surface Co/Al ratios were evaluated and compared as follows. Bulk and surface Co/Al ratios for the reference Co_2Mo_{10}/Al_2O_3 catalyst were 0.018 and 0.045, respectively. The bulk Co/Al ratio increased from 0.018 to 0.119 and the surface Co/Al ratio increased from 0.045 to 0.144 with cobalt addition to support up to 8 wt.%. The surface ratios are higher than bulk ones for all prepared materials. The surface Co/Al ratio is three times higher than bulk one for the reference catalyst and catalyst supported on alumina with 2.1 wt.% Co loading. The catalyst prepared with alumina modified with maximum amount of Co has nearly equal surface (0.144) and bulk (0.119) Co/Al ratios. This can be viewed as evidence of the partly migration of cobalt into alumina at high loadings. The migrated Co particles (most likely, cobalt spinel) undergo sulfidation with difficulty and consequently, lose their action in catalysis.

Analysis of HRTEM micrographs shows that the increase of Co content in alumina led to a slight increase in stacking number (Table 3). Such little changes may be explained by weakening the interaction between active phase and modified support [28], and should not have significant effect on catalytic activity of $Co_2Mo_{10}/Co_x/Al_2O_3$ catalysts. It was impossible to detect Co_9S_8 crystallites on HRTEM micrographs, in spite of appreciable quantity of cobalt sulphide in $Co_2Mo_{10}/Co_{8.3}/Al_2O_3$ sample.

The constancy of active phase composition was confirmed by XPS (Table 2). The values of $(Co/Mo)_{slab}$ and $(Co/Mo)_{edge}$ for all the prepared catalysts stayed approximately constant. It should be noted that $(Co/Mo)_{slab}$ value was constantly 0.2 that corresponds to Co/Mo ratio in the precursor – $Co_2Mo_{10}Am$. Meanwhile, with the increase of Co loading, the value of $(Co/Mo)_{tot}$ also increased from 0.23 to 1.14. It eliminates the possibility of cobalt migration from Co_9S_8 to CoMoS phase during the activation procedure before testing.

Such results indicate that composition and promotion degree of formed CoMoS active phase on the catalyst surface are the same for all samples. It was also confirmed by the similar relative distribution of molybdenum on catalysts surface (Table 2). The change of cobalt distribution can be explained by Co_9S_8 phase formation on modified alumina. That resulted in the decline of the relative content of cobalt in CoMoS phase due to the increase of total Co loading in $Co_2Mo_{10}/Co_x/Al_2O_3$ catalysts.

It has been shown that the morphology and composition of the active phase were constant. The packing density of the CoMoS phase crystallites on the catalyst surface (m value) varies between 44 and 51 MoS_2 crystallites per 1000 nm^2 with cobalt addition to alumina. This accords with the same Mo loading in prepared catalysts, the same average length and stacking number of the formed CoMoS phase and nearly equal values of SSA. The TOF value was used to evaluate the result of alumina modifying by cobalt on catalytic properties of the catalysts. The spillover effect (synergism factor) based on TOF value (Eq. (16)) was also introduced to assess this effect numerically. The efficiency of $Co_2Mo_{10}/Co_x/Al_2O_3$ catalysts with a considerable amount of cobalt sulphide is higher than the efficiency of the reference one (Co_2Mo_{10}/Al_2O_3) and the catalyst modified with a small amount of cobalt.

To describe the catalytic behavior of CoMo-catalysts in HDS reactions it is preferable to use adjusted values of turnover frequency (TOF$^{/}$) with allowance for stacking number of CoMoS active phase particles (Eq. (14)) as it was shown previously in [26] for alumina-supported CoMo-catalysts. It was also reported that TOF$^{/}$value is lineally dependent on average length ($\bar{L}$) of the active phase crystallites (Fig. 4 dash line) [26]. The results of DBT HDS over $Co_2Mo_{10}/Co_x/Al_2O_3$ catalysts (Fig. 4 light diamonds) are within the range of 2.6–2.9 nm on a diagram. Fig. 4 shows that catalysts with equal Mo loading, precursor and morphology of the active phase and differ only in Co_9S_8 phase content on the surface demonstrate big difference in catalytic properties in DBT HDS. $Co_2Mo_{10}/Co_{8.1}/Al_2O_3$ catalyst with high amount of Co_9S_8 demonstrated the same activity (Fig. 4 point «8.1%») at 275 °C as it was

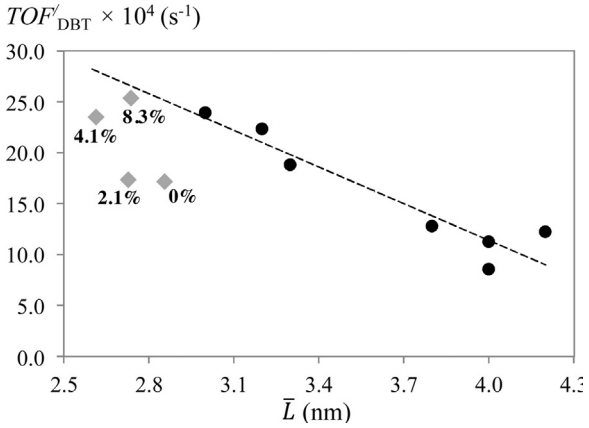

Fig. 4. Dependence of the TOF$^{/}$value of DBT HDS over $Co_2Mo_{10}/Co_x/Al_2O_3$ catalysts on CoMoS phase morphology. ◊(gray) – this work results (T = 275 °C), ● – adapted from [26] (T = 300 °C).

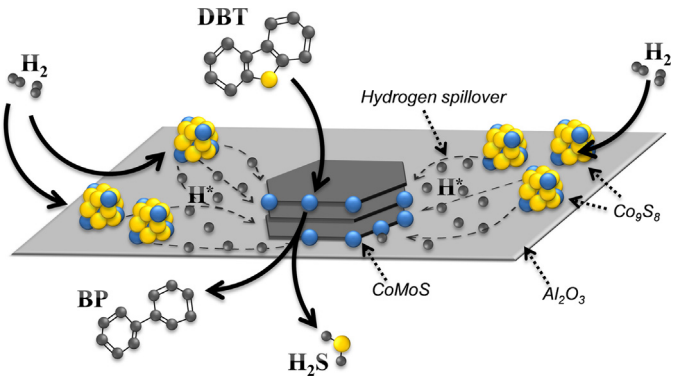

Fig. 5. Proposed model of DBT HDS reaction on $Co_2Mo_{10}/Co_x/Al_2O_3$ catalysts involving hydrogen spillover.

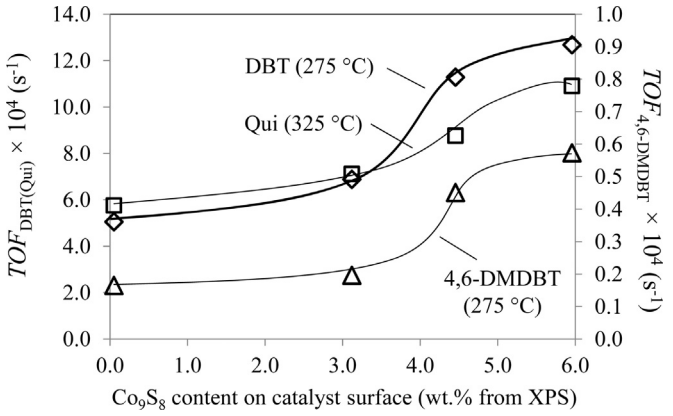

Fig. 6. Dependence of TOF values of DBT and 4,6-DMDBT HDS (at 275 °C, 40 h^{-1}) and Qui HDN (at 325 °C, 20 h^{-1}) reactions over $Co_2Mo_{10}/Co_x/Al_2O_3$ catalysts on Co_9S_8 content.

obtained at 300 °C on no-modified catalyst previously (Fig. 4 dash line). This result corresponds to evaluated value of spillover effect ($SE^{/TOF}$) that is about 1.5. This outcome is cautiously interpreted in favor of spillover effect due to cobalt sulphide ability to accumulate and activate molecular hydrogen to monatomic, presumably according to a heterolytic type of bond breaking [49,68]. Cobalt sulphide species located on the catalyst surface promote hydrogen spillover and modify the efficiency of CoMoS active sites in HDS of DBT. Fig. 5 shows a possible way of hydrogen migration from Co_9S_8 particles to HDS active sites located on CoMoS phase species.

The values of HYD/DDS selectivity for HDS of DBT make additional support for the spillover effect theory. $Sel_{HYD/DDS}$ ratios for the catalysts supported on Co_x/Al_2O_3 carriers are higher than selective ratio for the reference one. Increase of k_{HYD} rate constants can be caused by the hydrogen spillover provided by Co_9S_8 particles.

The same trends may be observed for the HDS of 4,6-DMDBT (Table 5). The increase of Co loading in support resulted in the growth of CoMoS active sites efficiency. TOF values increase more than twice with cobalt sulphide addition to alumina support. Reference TOF value is $0.13 \times 10^4\ s^{-1}$ while $Co_2Mo_{10}/Co_{8.3}/Al_2O_3$ catalyst demonstrate $0.47 \times 10^4\ s^{-1}$ TOF in 4,6-DMDBT HDS. $Co_2Mo_{10}/Co_x/Al_2O_3$ catalysts with Co content in alumina more than 4 wt.% demonstrate a considerable increase of TOF as well as spillover effect ($SE^{/TOF}$) exceeding 2.0 (Fig. 6). That happens due to the increase of hydrogenating activity which was confirmed by the 4,6-DMDBT HDS selectivity ratio. It grew from 5.5 to 7.5 with Co addition to alumina. Adjusted values of TOF and synergism effect for HDS of 4,6-DMDBT describe well the observed trends.

In case of Qui HDN, catalytic activity grew less than in HDS reactions. The extent of denitrogenation increased from 35 to 42% with cobalt addition to support, whereas TOF almost doubled (Table 6). It was shown that TOF and SE integral values (calculated using Eqs. (14) and (16)) corresponding to all the active sites, instead of multislab CoMoS particles only, are preferable to describe the effect of support modifying by cobalt on catalytic activity in Qui HDN. Such catalytic behavior can be attributed to the specific features of HDN reaction mechanism and as a result, cobalt sulphide particles had less influence on HDN reactions

The observed TOF values for $Co_2Mo_{10}/Co_x/Al_2O_3$ catalysts in HDS and HDN reactions were compared with published results in Table 7. Catalysts prepared with Co-modified alumina demonstrate much higher efficiency of CoMoS active sites (TOF values)

Table 7
Comparison of TOF values of CoMo and phosphide catalysts in various reactions.

Catalyst	Reactant	Reaction	Conditions	TOF ($\times 10^{-4}\ s^{-1}$)	Ref.
$Co_2Mo_{10}/Co_{8.3}/Al_2O_3$	DBT	HDS	Micro-reactor	25.4	This work
	4,6-DMDBT		T = 275 °C, P = 3.0 MPa	0.9	
	Quinoline	HDN	T = 325 °C, P = 3.0 MPa	21.8	
Co_2Mo_{10}/Al_2O_3	DBT	HDS	Micro-reactor	23.9	[26]
	4,6-DMDBT		T = 300 °C, P = 3.0 MPa	4.4	
Co_3[EDTA]–Co_2Mo_{10}/Al_2O_3	DBT			18.8	
	4,6-DMDBT			4.9	
Industrial catalyst	DBT	HDS	Autoclave	0.4	[70]
$CoMoS/Al_2O_3$			T = 300 °C, P = 2.0 MPa		
Industrial catalyst	DBT	HDS	Autoclave	0.4	[69]
$CoMoS/Al_2O_3$	4,6-DMDBT		T = 320 °C, P = 3.0 MPa	0.1	
$CoMo/Al_2O_3$	DBT	HDS	Autoclave	10.8	[71]
	4,6-DMDBT		T = 300 °C, P = 4.0 MPa	1.4	
CoMo/C	DBT			9.5	
	4,6-DMDBT			1.1	
CoMoS-S/γ-Al_2O_3	4,6-DMDBT	HDS	Micro-reactor	0.8	[72]
CoMoS-S/γT-Al_2O_3			T = 300 °C, P = 2.5 MPa	1.3	
CoMoS-S/δ-Al_2O_3				1.9	
$Co_{0.1}Ni_{1.9}P/SiO_2$	Carbazole	HDN	Micro-reactor	1.4	[75]
Sulf. Ni-Mo/Al_2O_3			T = 300 °C, P = 3.0 MPa	1.7	
CoP/SiO_2	DBT	HDS	Micro-reactor	8.1	[73]
	Quinoline	HDN	T = 370 °C, P = 3.1 MPa	12	
Ni_2P/SiO_2	DBT	HDS		15	
	Quinoline	HDN		6	
Bulk MoP	Carbazole	HDN	Micro-reactor	65.9	[74]
Bulk NiMoP			T = 310 °C, P_{H2} = 3.0 MPa	18.9	

Table 8
Spillover effect investigation of Donor (**D**)//Separator//Acceptor (**A**) catalytic systems in various reactions.

Catalytic system composition			Feedstock	Process conditions	T (°C)	Synergism factor[a]	Ref.
Donor (**D**)	Acceptor (**A**)	Separator					
Co_9S_8 Co = 4.1 wt.%	$CoMo/Al_2O_3$ Co = 1.6 wt.% Mo = 12.7 wt.%	–	DBT (1500 ppm S in toluene)	P = 3 MPa, LHSV = 40 h^{-1}, H_2/feedstock = 600 nL/L	250 275	1.72 1.58	This work
			4,6-DMDBT (300 ppm S in toluene)	(the same cond.)	275	2.2	
			Quinoline (750 ppm N in toluene)	LHSV = 20 h^{-1}	325	1.2	
Co/Al_2O_3 Co = 1.2 wt.%	Mo/Al_2O_3 Mo = 10 wt.%	SiO_2	DBT (1500 ppm S in toluene)	P = 3 MPa, LHSV = 50 h^{-1}, H_2/feedstock = 600 nL/L	300 325 350	1.38 1.14 1.09	[41]
$Co(Ni)/Al_2O_3$ Co(Ni)O = 3.9 wt.%	Mo/Al_2O_3 MoO_3 = 11.9 wt.%	SiO_2	DBT (2000 ppm DBT in decaline)	P = 3 MPa, LHSV = 30 h^{-1}, H_2/feedstock = 120 nL/L	325 350 375	1.26 (1.19) 1.08 (1.06) 1.05 (1.03)	[56]
Ru 1 wt.%	$NiMo/Al_2O_3$ ($CoMo/Al_2O_3$)	–	DBT (1 wt.% in decaline)	P = 3 MPa, LHSV = 35 h^{-1}, H_2/feedstock = 120 nL/L	280	1.5 (1.6)	[45]
Co/Al_2O_3 Co = 5.2 wt.%	Mo/Al_2O_3 Mo = 9.8 wt.%	SiO_2	Pre-treated Gas oil with ~0.02% S of 4-MDBT (4,6-DMDBT)	P_{H2} = 3 MPa, LHSV = 9 h^{-1}, H_2/feedstock = 400 nL/L	300	1.95 −2.29	[50]
Ni/Al_2O_3 NiO = 4 wt.%	Mo/Al_2O_3 MoO_3 = 18.1 wt.%	SiO_2	Quinoline (1000 ppm N in decaline)	P_{H2} = 2 MPa, LHSV = 3 h^{-1}, H_2/feedstock = 600 nL/L	280 300 320 340	1.32 1.28 1.27 1.06	[64]
Ni/Al_2O_3 NiO = 3.9 wt.%	Mo/Al_2O_3 MoO_3 = 11.9 wt.%	SiO_2	Pyridine (1000 ppm N in decaline)	P = 3 MPa, LHSV = 30 h^{-1}, H_2/feedstock = 120 nL/L	225 250	1.8 1.5	[48]
			Mixture of Gas-oil and pyridine (2000 ppm N)		275 325 350 375	1.3 1.7 1.5 1.1	
Co/SiO_2 CoO = 2 wt.%	Mo/SiO_2 MoO_3 = 8 wt.%	SiO_2	Gas oil (470 ppm S)	P = 3 MPa, LHSV = 9 h^{-1}, H_2/feedstock = 400 nL/L	325 350 375	1.7 1.5 1.4	[54]
Co/Al_2O_3 CoO = 3.9 wt.%		$Al_2O_3(SiO_2)$	Gas oil (5400 ppm S) MoO_3 = 11.9 wt.%	P = 3 MPa, LHSV = 9 h^{-1}, H_2/feedstock = 400 nL/L	325 350 375	1.26 (1.90) 1.16 (1.40) 1.08 (1.18)	[53]
$Co(Ni)/Al_2O_3$ Co(Ni) = 5.2 wt.%	Mo/Al_2O_3 Mo = 9.8 wt.%	SiO_2 LHSV = 9 h^{-1}, H_2/feedstock = 400 nL/L	Gas oil (2700 ppm S)	P = 3 MPa,	325 350 375	2.8 (2.8) 2.2 (2.3) 1.6 (1.5)	[49]

[a] Synergism factor calculated with Eq. (15).

than industrial ones [69,70] as well as catalysts supported on alumina and activated carbon [71] or various types of alumina using different Co precursors and preparation methods [72]. Comparison of obtained results with our previous experiments [26] shows that alumina support modifying with cobalt sulphide allows to obtain the same TOF in DBT HDS on CoMo active site at 25 °C less than the reference. The $Co_2Mo_{10}/Co_{8.1}/Al_2O_3$ catalyst exhibits activity in HDN reaction at operating conditions comparable with the results obtained on silica supported Co and Ni phosphates at 370 °C [73] and much higher than TOF values of carbazole HDN [74,75] due to steric constraints of tricyclic compounds.

Thus, the results obtained suggest high efficiency of the active sites formed from Co_2Mo_{10}HPA simultaneously with cobalt sulphide particles arranged on the surface of the catalysts. Therefore, the proposed approach of alumina support modifying can be used to prepare HDT catalysts with improved catalytic activity and stability on coke-on-catalyst production reactions and longer catalyst cycle length.

Results published on the synergetic effect investigation caused by hydrogen spillover over transition metal sulphides are summarized in Table 8. A stacked bed reactor with monometallic catalysts is usually used to prevent the formation of mixed phase and evaluate the synergism effect of hydrogen spillover [48–50,53,54,56,64]. The synergism factor calculated by Eq. (15) was used in all references. In order to compare the obtained results with published ones, the spillover effect presented in Table 8 was also calculated using Eq. (15). In all references, the value of spillover effect decreases with the increase of process temperature that arises from physical nature of adsorption phenomena. The presence of cobalt sulphide particles on the surface of $Co_2Mo_{10}/Co_{8.1}/Al_2O_3$ catalyst provide the significant synergetic effect in catalytic activity that is higher than values published for HDS reaction earlier [56] and our previous results [41] carried out with stacked bed catalysts. Comparable results were presented by Navarro et al. [45] for sulfide Ni(Co)Mo/Al_2O_3 catalysts doped with 1 wt.% of Ru. In the case of 4,6-DMDBT HDS, more essential effect of hydrogen spillover over $Co_2Mo_{10}/Co_x/Al_2O_3$ catalysts led to 2.2 times increase of TOF value. The importance of observed effect in the HDS reactions of hard-to-remove sulphur-containing compound was noted earlier [50]. The synergism effect observed in HDN of Qui over the $Co_2Mo_{10}/Co_{8.1}/Al_2O_3$ catalyst corresponds to the published results [48,64].

The obtained results emphasize the role of cobalt sulphide particles on catalysts surface. The sufficient quantity of Co_9S_8 species on the catalyst surface can play the role of a donor of activated hydrogen and have a positive effect on the efficiency of CoMoS active sites in the hydrogenolysis of heterocyclic compounds.

5. Conclusion

$Co_2Mo_{10}/Co_x/Al_2O_3$ catalysts synthesized using Co_2Mo_{10}Am and Co-modified alumina had equal morphology, composition and promotion degree of the formed CoMoS active phase. Prepared samples differed from each other only in Co_9S_8 phase concentration on their surfaces, which increased with cobalt addition to the support. That is why, the investigation of the role of cobalt sulphide particles in HDT catalysts became possible.

It was shown that highly dispersed cobalt sulphide particles located on the catalysts surface exerts beneficial effect on the catalytic properties of $Co_2Mo_{10}/Co_x/Al_2O_3$ catalysts.

- The catalysts revealed high activity in HDS of DBT and 4,6-DMDBT, furthermore the value of synergism effect for $Co_2Mo_{10}/Co_{8.1}/Al_2O_3$ sample reached 1.6 in DBT HDS and 2.1 in 4,6-DMDBT HDS.
- Cobalt addition to the catalyst support also increased activity of the $Co_2Mo_{10}/Co_x/Al_2O_3$ catalysts in Qui HDN reaction. Catalysts containing a considerable amount of cobalt sulphide demonstrate higher TOF values and Qui conversions.
- $Co_2Mo_{10}/Co_x/Al_2O_3$ catalysts exhibit higher HYD/DDS selectivity in HDS reactions that can be derived from hydrogen spillover effect provided by Co_9S_8 particles arranged on the catalyst support surface. Enhanced hydrogenating catalytic activity can be applied to prepare new HDT catalysts with improved catalytic activity and stability on coke-on-catalyst production reactions and longer catalyst cycle length.

It was proposed to evaluate the spillover effect value in supported catalysts as an increment of the TOF (SE^{TOF}) of reactions on promoted CoMoS sites due to presence of Co_9S_8 species. Obtained results make it possible to reassess the role of cobalt sulphide particles in HDT catalysts. The sufficient quantity of Co_9S_8 particles located on the catalysts surface can play the role of a donor of activated hydrogen, which can spill over to CoMoS active phase species over alumina surface and, thereby, increases TOF of the reactions. Therefore, cobalt sulphide entities have a positive effect on the efficiency of promoted CoMoS active sites in hydrogenolysis of heterocyclic compounds. Determined enhancements of the TOF values of HDS, HYD and HDN reactions on CoMoS sites are useful for developing new highly effective catalytic materials.

Acknowledgments

The authors thank Dr. K.I. Maslakov (Moscow State University) for the XPS measurements.

Al.A. Pimerzin thanks Haldor Topsøe Company for the grant to perform his PhD paper (2012–2014). The work was supported by Ministry of Education and Science of Russian Federation (project No. 2014/199).

References

[1] I.V. Babich, J.A. Moulijn, Fuel 82 (2003) 607–631.
[2] E. Loury, The Los Angeles Times, 2012.
[3] http://www.epa.gov/otaq/fuels/dieselfuels/index.htm
[4] http://www.dieselnet.com/
[5] http://ec.europa.eu/enterprise/automotive/directives/vehicles/index.htm
[6] S.T. Oyama, T. Gott, H. Zhao, Y.-K. Lee, Catal. Today 143 (2009) 94–107.
[7] A. Stanislaus, A. Marafi, M.S. Rana, Catal. Today 153 (2010) 1–68.
[8] H. Toulhoat, P. Raybaud, Catalysis by Transition Metal Sulfides: From Molecular Theory to Industrial Application, Eíditions TECHNIP, Lionbridge, Paris, 2013.
[9] Hydrotreating Catalysis-Science and Technology, in: H. Topsoe, B.S. Clausen, F.E. Massoth (Eds.), Springer Verlag, Berlin, 1996.
[10] H. Topsøe, Appl. Catal. A 322 (2007) 3–8.
[11] E.J.M. Hensen, V.H.J. de Beer, J.A.R. van Veen, R.A. van Santen, Catal. Lett. 84 (2002) 59–67.
[12] M. Breysse, C. Geantet, P. Afanasiev, J. Blanchard, M. Vrinat, Catal. Today 130 (2008) 3–13.
[13] T.A. Zepeda, B. Pawelec, J.N. Díaz de León, J.A. de los Reyes, A. Olivas, Appl. Catal. B: Environ. 111–112 (2012) 10–19.
[14] S. Sawhill, K. Layman, D. Vanwyk, M. Engelhard, C. Wang, M. Bussell, J. Catal. 231 (2005) 300–313.
[15] M. Nagai, Appl. Catal. A 322 (2007) 178–190.
[16] A. Montesinos-Castellanos, T.A. Zepeda, B. Pawelec, E. Lima, J.L.G. Fierro, A. Olivas, J.A. de los Reyes, Appl. Catal. A 334 (2008) 330–338.
[17] P. Blanchard, C. Lamonier, A. Griboval, E. Payen, Appl. Catal. A 322 (2007) 33–45.
[18] A.A. Spojakina, K. Jiratova, G. Kostova, J. Kocianova, M. Stamenova, Kinet. Catal. 44 (2003) 886–892.
[19] A.A. Spojakina, E.U. Kraleva, K. Jiratova, J. Kocianova, L.A. Petrov, $FePMo_{12}O_{40}$ Heteropolycompound in Preparation of Hydrodesulfurization Catalysts, Bulgarian Academy of Sciences, Sofia, Bulgarie, 2002.
[20] N.N. Tomina, P.A. Nikulshin, A.A. Pimerzin, Pet. Chem. 48 (2008) 92–99.
[21] C.I. Cabello, I.L. Botto, H.J. Thomas, Appl. Catal. A 197 (2000) 79–86.
[22] C.I. Cabello, M. Muñoz, I.L. Botto, E. Payen, Thermochim. Acta 447 (2006) 22–29.
[23] C.I. Cabello, M. Munoz, E. Payen, H.J. Thomas, Catal. Lett. 92 (2004) 69–73.

[24] C. Lamonier, C. Martin, J. Mazurelle, V. Harlé, D. Guillaume, E. Payen, Appl. Catal. B: Environ. 70 (2007) 548–556.
[25] N.N. Tomina, P.A. Nikulshin, A.A. Pimerzin, Kinet. Catal. 49 (2008) 653–662.
[26] P.A. Nikulshin, D.I. Ishutenko, A.A. Mozhaev, K.I. Maslakov, A.A. Pimerzin, J. Catal. 312 (2014) 152–169.
[27] P.A. Nikulshin, A.A. Mozhaev, K.I. Maslakov, A.A. Pimerzin, V.M. Kogan, Appl. Catal. B: Environ. 158–159 (2014) 161–174.
[28] P.A. Nikulshin, A.A. Mozhaev, A.A. Pimerzin, V.V. Konovalov, Fuel 100 (2012) 24–33.
[29] P.A. Nikulshin, V.A. Salnikov, A.A. Mozhaev, P.P. Minaev, V.M. Kogan, A.A. Pimerzin, J. Catal. 309 (2014) 386–396.
[30] P.A. Nikul'shin, A.V. Mozhaev, D.I. Ishutenko, P.P. Minaev, A.I. Lyashenko, A.A. Pimerzin, Kinet. Catal. 53 (2012) 620–631.
[31] P.A. Nikul'shin, A.V. Mozhaev, A.A. Pimerzin, N.N. Tomina, V.V. Konovalov, V.M. Kogan, Kinet. Catal. 52 (2011) 862–875.
[32] A.A. Mozhaev, P.A. Nikul'shin, A.A. Pimerzin, V.V. Konovalov, A.A. Pimerzin, Pet. Chem. 52 (2012) 45–53.
[33] P.A. Nikulshin, N.N. Tomina, A.A. Pimerzin, A.Y. Stakheev, I.S. Mashkovsky, V.M. Kogan, Appl. Catal. A 393 (2011) 146–152.
[34] J. Mazurelle, C. Lamonier, C. Lancelot, E. Payen, C. Pichon, D. Guillaume, Catal. Today 130 (2008) 41–49.
[35] C.I. Cabello, F.M. Cabrerizo, A. Alvarez, H.J. Thomas, J. Mol. Catal. A 186 (2002) 89–100.
[36] M. Rana, J. Ramirez, A. Gutierrezalejandre, J. Ancheyta, L. Cedeno, S. Maity, J. Catal. 246 (2007) 100–108.
[37] L. Coulier, V.H.J. de Beer, J.A.R. van Veen, J.W. Niemantsverdriet, J. Catal. 197 (2001) 26–33.
[38] R. Palcheva, L. KaluŽA, A. Spojakina, K. JirÁTovÁ, G. Tyuliev, Chin. J. Catal. 33 (2012) 952–961.
[39] R. Palcheva, A. Spojakina, L. Dimitrov, K. Jiratova, Microporous Mesoporous Mater. 122 (2009) 128–134.
[40] R. Palcheva, A. Spojakina, G. Tyuliev, K. Jiratova, L. Petrov, Kinet. Catal. 48 (2007) 847–852.
[41] A.A. Pimerzin, P.A. Nikulshin, A.V. Mozhaev, A.A. Pimerzin, Pet. Chem. 53 (2013) 245–254.
[42] L. Ding, Z. Zhang, Y. Zheng, Z. Ring, J. Chen, Appl. Catal. A 301 (2006) 241–250.
[43] T. Klimova, P.M. Vara, I.P. Lee, Catal. Today 150 (2010) 171–178.
[44] S. Maity, G. Flores, J. Ancheyta, M. Rana, Catal. Today 130 (2008) 374–381.
[45] R.M. Navarro, P. Castaño, M.C. Álvarez-Galván, B. Pawelec, Catal. Today 143 (2009) 108–114.
[46] Y. Saih, K. Segawa, Appl. Catal. A 353 (2009) 258–265.
[47] V. Sundaramurthy, A.K. Dalai, J. Adjaye, Appl. Catal. A 335 (2008) 204–210.
[48] F. Valdevenito, R. García, N. Escalona, F.J. Gil-Llambias, S.B. Rasmussen, A. López-Agudo, Catal. Commun. 11 (2010) 1154–1156.
[49] M. Villarroel, P. Baeza, N. Escalona, J. Ojeda, B. Delmon, F.J. Gil-Llambías, Appl. Catal. A 345 (2008) 152–157.
[50] M. Villarroel, E. Camú, N. Escalona, P. Ávila, S.B. Rasmussen, P. Baeza, F. Gil-Llambías, Appl. Catal. A 399 (2011) 63–68.
[51] M. Villarroel, A. Méndez, G. Águila, N. Escalona, P. Baeza, F. Gil-Llambías, Catal. Today 156 (2010) 65–68.
[52] M. Boudart, M.A. Vannice, J.E.Z. Benson, Phys. Chem. Neue Folge 64 (1969) 171.
[53] P. Baeza, M.S. Ureta-Zañartu, N. Escalona, J. Ojeda, F.J. Gil-Llambías, B. Delmon, Appl. Catal. A 274 (2004) 303–309.
[54] J. Ojeda, N. Escalona, P. Baeza, M. Escudey, F.J. Gil-Llambas, Chem. Commun. (2003) 1608.
[55] P. Baeza, M. Villarroel, P. Ávila, A. López Agudo, B. Delmon, F.J. Gil-Llambías, Appl. Catal. A 304 (2006) 109–115.
[56] N. Escalona, R. García, G. Lagos, C. Navarrete, P. Baeza, F.J. Gil-Llambías, Catal. Commun. 7 (2006) 1053–1056.
[57] M. Villarroel, P. Baeza, F. Gracia, N. Escalona, P. Avila, F.J. Gil-Llambías, Appl. Catal. A 364 (2009) 75–79.
[58] A.N. Varakin, P.A. Nikul'shin, A.A. Pimerzin, V.A. Sal'nikov, A.A. Pimerzin, Russ. J. Appl. Chem. 86 (2013) 718–726.
[59] E. Schill, Iso-und Heteropolyverbindungen, F. Enke (Ed.) Verlag, Stuttgart, 1981.
[60] P.A. Nikulshin, N.N. Tomina, A.A. Pimerzin, A.V. Kucherov, V.M. Kogan, Catal. Today 149 (2010) 82–90.
[61] S. Kasztelan, H. Toulhoat, J. Grimblot, J.P. Bonnelle, Appl. Catal. 13 (1984) 127.
[62] A.D. Gandubert, E. Krebs, C. Legens, D. Costa, D. Guillaume, P. Raybaud, Catal. Today 130 (2008) 149–159.
[63] A.D. Gandubert, C. Legens, D. Guillaume, S. Rebours, E. Payen, Oil Gas Sci. Technol.–Revue de l'IFP 62 (2007) 79–89.
[64] L. Liu, B. Liu, Y. Chai, Y. Liu, C. Liu, J. Nat. Gas Chem. 20 (2011) 214–217.
[65] I. Alstrup, I. Chorkendorff, R. Candia, B.S. Clausen, H. Topsøe, J. Catal. 77 (1982) 397–409.
[66] A.M. de Jong, V.H.J. de Beer, J.A.R. van Veen, J.W. Niemantsverdriet, J. Phys. Chem. 100 (1996) 17722–17724.
[67] J.C. Dupin, D. Gonbeau, I. Martin-Litas, P. Vinatier, A. Levasseur, Appl. Surf. Sci. 173 (2001) 140–150.
[68] M. Breysse, E. Furimsky, S. Kasztelan, M. Lacroix, G. Perot, Catal. Rev. 44 (2002) 651–735.
[69] M. Kouzu, K. Uchida, Y. Kuriki, F. Ikazaki, Appl. Catal. A 276 (2004) 241–249.
[70] J.H. Kim, X. Ma, C. Song, Y.-K. Lee, S.T. Oyama, Energy Fuels 19 (2005) 353–364.
[71] J.J. Lee, S. Han, H. Kim, J.H. Koh, T. Hyeon, S.H. Moon, Catal. Today 86 (2003) 141–149.
[72] D. Laurenti, B. Phung-Ngoc, C. Roukoss, E. Devers, K. Marchand, L. Massin, L. Lemaitre, C. Legens, A.-A. Quoineaud, M. Vrinat, J. Catal. 297 (2013) 165–175.
[73] X. Wang, P. Clark, S.T. Oyama, J. Catal. 208 (2002) 321–331.
[74] I.I. Abu, K.J. Smith, Catal. Today 125 (2007) 248–255.
[75] R.H. Bowker, B. Ilic, B.A. Carrillo, M.A. Reynolds, B.D. Murray, M.E. Bussell, Appl. Catal. A 482 (2014) 221–230.